Towards scalable perovskite-based multijunction solar modules

Manoj Jaysankar*[a, b], Stefan Paetel[c], Erik Ahlswede[c], Ulrich W. Paetzold[d], Tom Aernouts[a], Robert Gehlhaar[a], Jef Poortmans[a, b]

a. IMEC – Partner in Solliance, Kapeldreef 75, 3001 Leuven, Belgium

b. Department of Electrical Engineering, KU Leuven, 3001 Leuven, Belgium

c. Zentrum für Sonnenenergie- und Wasserstoff-Forschung Baden-Württemberg (ZSW), 70563 Stuttgart, Germany

d. Institute of Microstructure Technology, Karlsruhe Institute of Technology, 76344 Eggenstein-Leopoldshafen, Germany

* Corresponding author: manoj.jaysankar@imec.be

Abstract

Perovskite-based multijunction solar cells can potentially overcome the power conversion efficiency (PCE) limits of established solar cell technologies. The technology combines high-efficiency perovskite top solar cells with crystalline silicon (c-Si) and copper indium gallium diselenide (CIGS) single junction solar cells enabling a more efficient harnessing of solar energy. In this work, we present high-efficiency and scalable perovskite-CIGS and perovskite-Si multijunction solar modules in a four-terminal configuration. We design the multijunction solar modules for minimal optical losses through careful optical engineering. In addition to optimised light coupling, the solar modules are fabricated in a scalable device design. Starting form lab-scale cells of 0.13 cm^2, we scale up the multijunction devices by two orders of magnitude to 16 cm^2 and investigate the various losses affecting the PCE of large-area multijunction solar modules, thus providing valuable insights into scalability of the technology. The champion perovskite-CIGS and perovskite-Si multijunction solar modules exhibit higher PCE than the stand-alone devices on sizes up 16 cm^2, paving the way for high-effiency perovskite-based multijunction photovoltaics. This work brings to forth relevant upscaling aspects of perovskite-based multijunction solar cell technology which is a key milestone in the road to commercial feasibility of the perovskite-based multijunction solar cell technology.

Keywords: Perovskite, Multijunction, Thin film tandems, Scalability

Introduction

Perovskite photovoltaic (PV) technology has demonstrated remarkable advancement in recent years reaching power conversion efficiencies (PCEs) comparable to established PV technologies such as single-junction crystalline silicon (c-Si) and copper indium gallium diselenide (CIGS).(*1*) Moreover, remarkable electronic properties coupled with simple, inexpensive fabrication make perovskite solar cells ideal candidates for low-cost, high-efficient multi-junction photovoltaics.(*2*–*7*) Multijunction solar cells such as perovskite-si and perovskite-CIGS hold the exciting potential to surpass the theoretical efficiency limits of commercial single-junction solar cells.(*8*–*13*)

Perovskite-based multijunction solar cells come in two different flavours: two-terminal and four-terminal. In two-terminal or monolithic devices, the top and bottom sub cells are serially connected. As a result, the cell producing the lower current in the system determines the overall current output thus requiring current matching of both sub cells for optimum operation. This characteristic of two-terminal multijunction solar cells influences their overall energy yield under non-standard spectral conditions and when the bandgaps of the sub cells are not optimal.(*14*, *15*) The four-terminal configuration circumvents this issue of current matching by electrically isolating the top and bottom sub cells. This configuration allows for independent optimization of the sub cells as well as modular fabrication. However, the four-terminal configuration needs two transparent electrodes, which could result in additional parasitic absorption. Additionally, since the output power will be extracted independently from the top and bottom sub cells, additional inverters, cabling and connectors will be required leading to increased complexity. On the flipside, it also results in reduced influence of spectral variations on the overall energy yield of the multijunction solar cell.(*15*, *16*)

In recent years, significant advances in lab-scale multijunction PCE have been reported, abundantly for perovskite-Si and modestly for perovskite-CIGS multijunction solar cells.(*5*, *7*, *17*–*23*) The prospect of scalable high-efficient perovskite-Si and perovskite-CIGS multijunction solar modules hold substantial potential for a disruptive change in the PV market.(*24*, *25*) Intrinsic electrical characteristics, optics of the layer stack, effectiveness of deposition techniques, all have significant impact on the overall performance of the multijunction devices.(*26*–*29*) Recently, an all-thinfilm monolithic perovskite-CIGS multijunction solar cell with PCE of 21.6% on 0.8 cm^2 was demonstrated.(*30*) Such advances demonstrate the attractive prospects of all-thinfilm perovskite-CIGS multijunction solar cells. Moving away from small-area lab-scale cells, the difference in PCE of solar modules and solar cell for such multijunction devices exposes the issues with scalability of this technology to commercial dimensions.(*17*, *18*, *31*, *32*)

In this work, we examine the scalability of four-terminal perovskite-Si and perovskite-CIGS multijunction solar cells while maintaining high aperture PCE. Using an efficient module design, we scale up the multijunction devices from 0.13 cm^2 to 16 cm^2 aperture area. By upgrading the device architecture from cell level to module level, a smooth transition towards large-scale modules is denoted. Additionally, designs with

minimal optical losses of the perovskite-Si and perovskite-CIGS multijunction layer stacks are realized. By reducing parasitic absorption and enhancing near-infrared transmittance, we boost light coupling between perovskite and Si/CIGS devices leading to significant enhancement in overall PCE of the multijunction solar modules. Besides scaling up the perovskite devices by two orders of magnitude, we provide detailed analysis of efficiency loss when scaling up, thus bringing to forth relevant upscaling aspects of perovskite-based multijunction solar cell technology.

Results and Discussion

Perovskite solar cells are commonly fabricated on glass substrates with a pre-deposited, high-conductive commercial ITO layer. The layer stack of our reference semi-transparent perovskite solar cell is shown in Figure 1a. It consists of a glass substrate coated with commercial indium tin oxide (ITO), planar TiO_2, $Cs_{0.1}FA_{0.9}PbI_{2.865}Br_{0.135}$ perovskite absorber, Spiro-OMeTAD, MoO_3, and in-house ITO. We minimize front reflection at the air-glass interface by using an antireflective textured foil as described in our earlier work.(*19*)

The 150 nm thick commercial ITO, which is the front transparent electrode in our reference perovskite solar cell has a sheet resistance of ~15 Ω/□. The low sheet resistance translates to high lateral conductivity of the layer. On the flipside, extinction coefficient of the commercial ITO layer is $\sim 10^{-2} - 10^{-1}$ in the near infrared (NIR) spectral region (800 nm – 1200 nm), which results in parasitic absorption and significant optical losses in perovskite-Si and perovskite-CIGS multijunction devices (Table 1). The average NIR transmittance of our reference perovskite solar cell is 67%. The 100 nm thick in-house ITO functioning as the rear transparent electrode in the reference stack has an extinction coefficient one order of magnitude smaller than the commercial ITO. The transmittance of the ITO layers in the NIR spectral region is determined largely by free-carrier absorption. The in-house ITO has fewer free carriers than commercial ITO and hence less free-carrier absorption. This results in the in-house ITO having better NIR transmittance than commercial ITO. However, the fewer free carriers in the in-house ITO also results in higher sheet resistance of this layer (~70 Ω/□) compared to commercial ITO (~15 Ω/□). With a view to minimizing the parasitic absorption in the multijunction devices, we replace the commercial ITO with our in-house ITO for the front electrode (Figure 1b). In order to optimize transmittance and resistance while achieving good quality ITO, customized parameters were used for sputtering the in-house ITO (Details in the experimental methods section). The perovskite solar cell employing in-house ITO for both front and rear electrodes exhibits an average NIR transmittance of 82%, considerably higher than the reference owing to reduced parasitic absorption (Figure 2).

To achieve high multijunction PCE, it is crucial to ensure that a high percentage of NIR light not absorbed by the perovskite top solar cell is transmitted to the bottom solar cell for absorption. In addition to the transmittance of the ITO layer, the transmittance of the perovskite solar cell is influenced by the intermediate medium between the perovskite and the bottom solar cells. One of the approaches to improve the NIR transmittance is to optimize the index of refraction of the intermediate medium through commercially available refractive index matching liquids. Although the use of such customized liquids as intermediate medium can boost the transmittance of the perovskite top solar cell, practical integration of such liquid layers is complicated due to mechanical instabilities. A more robust solution to enhance the NIR transmittance of the perovskite solar cell while keeping air as the intermediate medium is by adding a layer of MgF_2 on the rear side of the perovskite top solar cell (Figure 1c).(*7*) Our ray-tracing simulations predict that introducing a layer of MgF_2 at the rear ITO–air interface has similar effect on the short-circuit current density (J_{SC}) of the silicon bottom solar cell as changing the refractive index of the intermediate medium (Figure 3). The MgF_2 layer reduces the gradient of refractive index from ITO to air, thus enhancing light transmission through the perovskite top solar cell (Figure 2). The optimum thickness of the MgF_2 layer for our multijunction layer stack is ~200 nm (Figure S1). This design allows for air to be the intermediate medium, making practical integration of the two sub cells easier while maximizing the transmittance of the perovskite solar cell. The average NIR transmittance of our perovskite solar cell with an optimally thick rear MgF_2 layer is 90% (Figure 2). Figure 4a shows the current-voltage characteristics of the semi-transparent perovskite solar cell with in-house ITO electrodes and MgF_2. The enhanced NIR transmittance of the perovskite top solar cell directly correlates to high EQE of the silicon and CIGS bottom solar cells (Figure 4b). In the cell-on-cell architecture with an aperture area of 0.13 cm^2, the overall multijunction PCE of the perovskite-CIGS solar cell is 23.8% and that of the perovskite-silicon solar cell is 26%, both significantly higher than the stand-alone PCE of the CIGS and silicon solar cells (Table S1). Detailed solar cell parameters are tabulated in Table 2.

Besides high-efficiency on small sizes, the scalability of such perovskite-based multijunction devices needs to be addressed for commercial viability of this technology. To that end, we fabricated perovskite-CIGS and perovskite-Si multijunction solar modules which are up to 2 orders of magnitude larger than the small-area cells. The key issue with fabrication of large-area multijunction solar modules lies with the scalability of the perovskite device. We investigated the losses in aperture PCE when scaling up the semitransparent perovskite device from 0.13 cm^2 cells to 4 cm^2 modules and further up to 16 cm^2 modules. The design of perovskite modules and choice of subcell widths (3 mm) are discussed in our earlier work.(*18*) We identify three loss factors, viz., resistance, dead area, and inhomogeneity. Resistance losses include loss in aperture PCE due to sheet resistance of the transparent electrodes and losses at interconnections of individual cell stripes in a module. Dead area losses are a consequence of the monolithic module design, where part of the active material is removed through scribes to allow interconnection of individual cell stripes. Dead area is the difference between aperture area and active area of a module. Inhomogeneity losses arise solely from the variation in uniformity of the layers deposited on

different sizes owing to increased probability of defects and low performing regions over larger areas.

Figure 5 illustrates the influence of the different loss factors on aperture PCE of the perovskite device when scaling up. The aperture PCE of a 0.13 sm^2 semitransparent perovskite cell is 16.7%, which reduces to 14.8% when scaled up to a 4 cm^2 module. The lowering of aperture PCE of the semitransparent perovskite device when going from a 0.13 cm^2 cell to a 4 cm^2 module is due to a combined effect of all three loss factors. We used a SPICE-based analog electronic circuit simulator to estimate the perovskite efficiency when scaling up from a 0.13 cm^2 cell to a 4 cm^2 mini-module comprising seven subcells each ~2.9 mm long.(*33*) Our estimate indicates that dead area loss accounts for ~58% of the difference in aperture PCE, while resistance loss constitutes ~31%. Our perovskite modules have a geometric fill factor of 0.91. In other words, 9% of the module aperture area is dead area, which justifiably makes dead area the major loss factor for aperture PCE when going from 0.13 cm^2 cell to 4 cm^2 module. The width of individual cell stripes in our perovskite solar module is optimized for the sheet resistance of ITO electrodes as described in our previous work,(*18*) thus minimizing the resistance loss when scaling up from cell to module. The 0.13 cm^2 perovskite cell and the 4 cm^2 perovskite mini-module are fabricated identically on substrates with identical dimensions. Hence, after accounting for resistance and dead area losses, the remaining loss in aperture PCE when going from 0.13 cm^2 cell to 4 cm^2 module is attributed to layer inhomogeneity, which accounts for 11% of the total losses. When scaling up the perovskite solar module from 4 cm^2 to 16 cm^2 with the same design, the aperture PCE decreases further from 14.8% to 12%. Since the percentage of dead area and the width of individual cell stripes are identical in 4 cm^2 and 16 cm^2 modules, we attribute the additional decrease in aperture PCE solely to inhomogeneity in the larger active area. We fabricated 16 cm^2 perovskite-Si multijunction solar module employing a 16 cm^2 monolithic perovskite solar module and four 4 cm^2 Si solar cells interconnected as a Si mini-module. Our 16 cm^2 perovskite-Si multijunction solar module exhibits an aperture PCE of 20.2% (Table 2).

Conclusion

Scalable perovskite solar modules have strong potential for low-cost, high-efficiency multijunction photovoltaics. Besides significantly boosting the PCE on 0.13 cm^2 cells, we have scaled up the perovskite-based multijunction devices up to 16 cm^2 while maintaining high PCE. Although the demonstrated multijunction module design is scalable to commercial dimensions, various factors affect the aperture PCE of such large-area modules. Resistive losses due to transparent electrodes can be reduced to a certain extent by using better conductive transparent electrodes such as hydrogen-doped indium oxide and indium zinc oxide.(*12*, *34*) Losses to aperture PCE due to dead area formed during patterning of the modules can be minimized by advanced laser patterning that improve the geometric fill factor.(*35*, *36*) We remark that while scaling up further industrial-scale modules, inhomogeneity will be the key loss factor limiting the aperture PCE of the perovskite solar module and consequently the multijunction solar module. Homogeneous, large-area perovskite coating and deposition techniques are therefore essential for maintaining the high aperture PCE on large sizes.(*37*, *38*) By combining comprehensive loss reduction strategies with effective large-area fabrication, perovskite-based multijunction solar modules with PCE surpassing established PV technologies can be realized on an industrial scale.

Acknowledgements

This work has been supported by Solliance, a partnership of R&D organizations from the Netherlands, Belgium and Germany working on thin-film photovoltaic solar energy. The authors declare no competing financial interests.

Notes and References

1. W. S. Yang *et al.*, *Science (80-.).* **356**, 1376–1379 (2017).
2. S. De Wolf *et al.*, *J. Phys. Chem. Lett.* **5**, 1035–1039 (2014).
3. S. D. Stranks *et al.*, *Science (80-.).* **342**, 341–344 (2013).
4. N. N. Lal *et al.*, *Adv. Energy Mater.* **7**, 1602761 (2017).
5. T. Duong *et al.*, *Adv. Energy Mater.* **7**, 1700228 (2017).
6. M. Jaysankar *et al.*, *J. Mater. Chem. A*. **4**, 10524–10531 (2016).
7. H. Shen *et al.*, *Energy Environ. Sci.* **11**, 394–406 (2018).
8. C. D. Bailie *et al.*, *Energy Environ. Sci.* **8**, 956–963 (2015).
9. I. Almansouri, A. Ho-Baillie, S. P. Bremner, M. A. Green, *IEEE J. Photovoltaics*. **5**, 968–976 (2015).
10. N. N. Lal, T. P. White, K. R. Catchpole, *IEEE J. Photovoltaics*. **4**, 1380–1386 (2014).
11. J. Werner *et al.*, *Sol. Energy Mater. Sol. Cells*. **141**, 407–413 (2015).
12. F. Fu *et al.*, *Nat. Commun.* **6**, 8932 (2015).
13. J. Werner, B. Niesen, C. Ballif, *Adv. Mater. Interfaces*. **5**, 1700731 (2018).
14. M. Bonnet-Eymard *et al.*, *Sol. Energy Mater. Sol. Cells*. **117**, 120–125 (2013).
15. U. W. Paetzold *et al.*, in *Light, Energy and the Environment* (OSA, Washington, D.C., 2016; https://www.osapublishing.org/abstract.cfm?URI=OSE-2016-SoW2C.4), p. SoW2C.4.
16. M. T. Hörantner, H. J. Snaith, *Energy Environ. Sci.* **10**, 1983–1993 (2017).
17. U. W. Paetzold *et al.*, *J. Mater. Chem. A*. **5**, 9897–9906 (2017).
18. M. Jaysankar *et al.*, *Adv. Energy Mater.* **7**, 1602807 (2017).
19. M. Jaysankar *et al.*, *Energy Environ. Sci.* **11**, 1489–1498 (2018).
20. F. Sahli *et al.*, *Adv. Energy Mater.* **8**, 1701609 (2018).
21. J. Werner *et al.*, *ACS Energy Lett.* **1**, 474–480 (2016).
22. D. Forgács *et al.*, *Adv. Energy Mater.* **7**, 1602121 (2017).
23. Y. Wu *et al.*, *Energy Environ. Sci.* **10**, 2472–2479 (2017).
24. I. M. Peters, S. Sofia, J. Mailoa, T. Buonassisi, *RSC Adv.* **6**, 66911–66923 (2016).
25. P. A. Basore, in *2016 IEEE 43rd Photovoltaic Specialists Conference (PVSC)* (IEEE, 2016;

http://ieeexplore.ieee.org/document/7750126/), pp. 2635–2637.
26. M. van Eerden *et al.*, *Adv. Opt. Mater.* **5**, 1700151 (2017).
27. M. Filipič *et al.*, *Opt. Express*. **23**, A263 (2015).
28. M. Jošt *et al.*, *ACS Photonics*. **4**, 1232–1239 (2017).
29. S. Manzoor *et al.*, *Sol. Energy Mater. Sol. Cells*. **173**, 59–65 (2017).
30. M. Jošt *et al.*, *ACS Energy Lett.* **4**, 583–590 (2019).
31. W. Qiu *et al.*, *Energy Environ. Sci.* **9**, 484–489 (2016).
32. W. Qiu *et al.*, *Adv. Funct. Mater.* **27**, 1700920 (2017).
33. S. Eidelloth, F. Haase, R. Brendel, *IEEE J. Photovoltaics*. **2**, 572–579 (2012).
34. J. Werner *et al.*, *Sol. Energy Mater. Sol. Cells*. **141**, 407–413 (2015).
35. F. Matteocci *et al.*, *Prog. Photovoltaics Res. Appl.* **24**, 436–445 (2016).
36. B. Turan, A. Huuskonen, I. Kühn, T. Kirchartz, S. Haas, *Sol. RRL*. **1**, 1700003 (2017).
37. Z. Yang, S. Zhang, L. Li, W. Chen, *J. Mater.* **3**, 231–244 (2017).
38. S. Razza, S. Castro-Hermosa, A. Di Carlo, T. M. Brown, *APL Mater.* **4**, 091508 (2016).

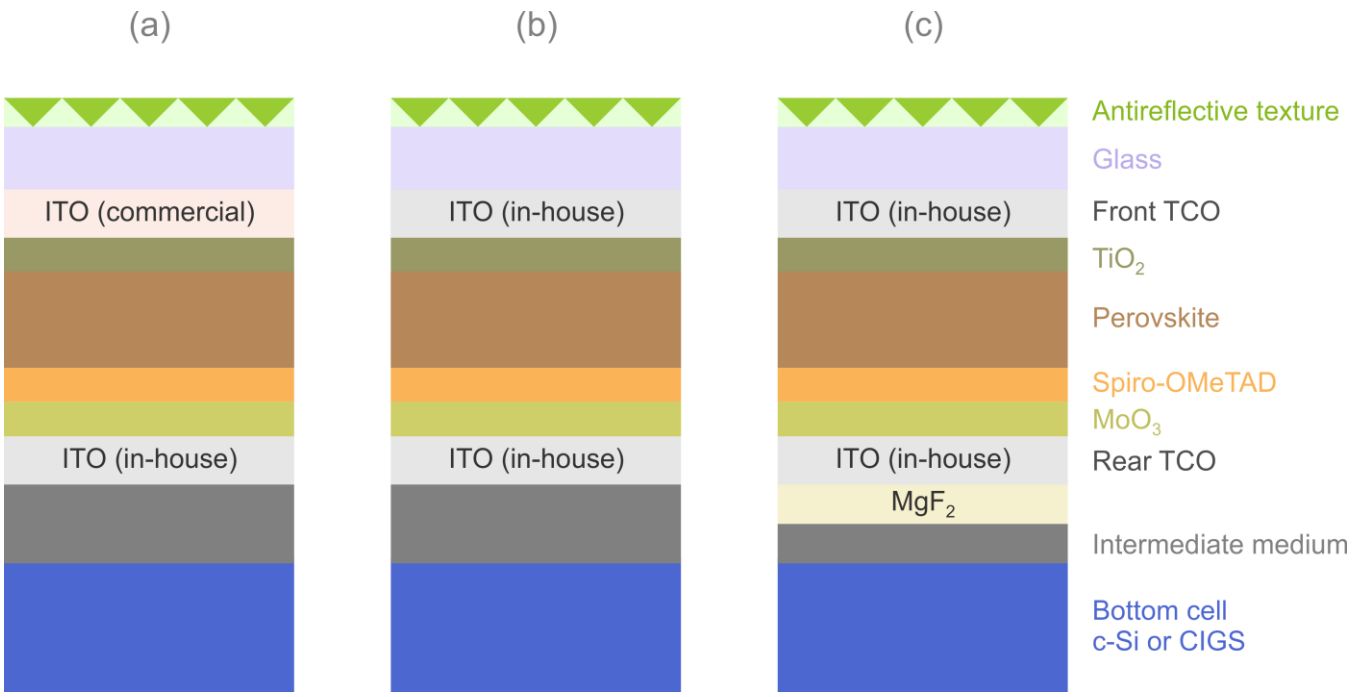

Figure 1 Schematic of multijunction solar cells for three cases with progressive light management.

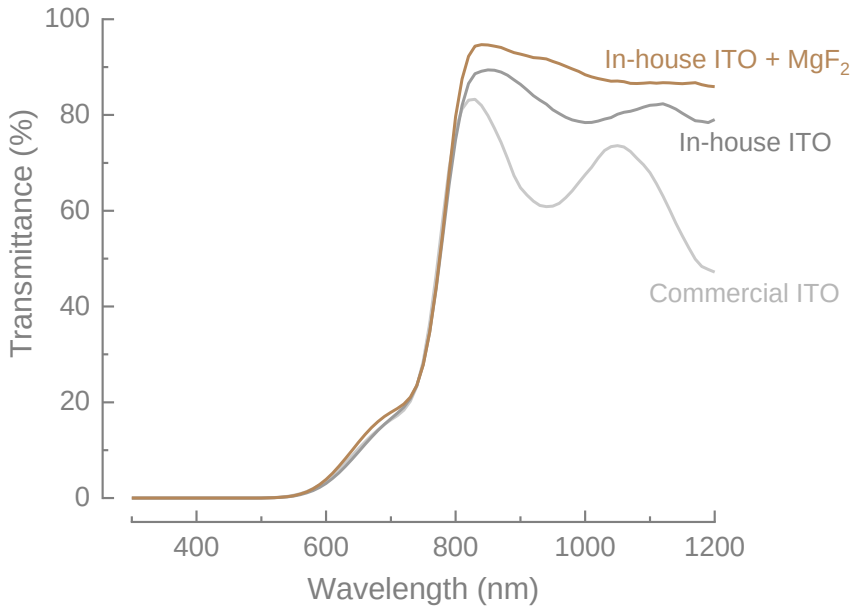

Figure 2 Measured transmittance of semitransparent perovskite solar cell to air for three cases with increasing near-infrared transmittance.

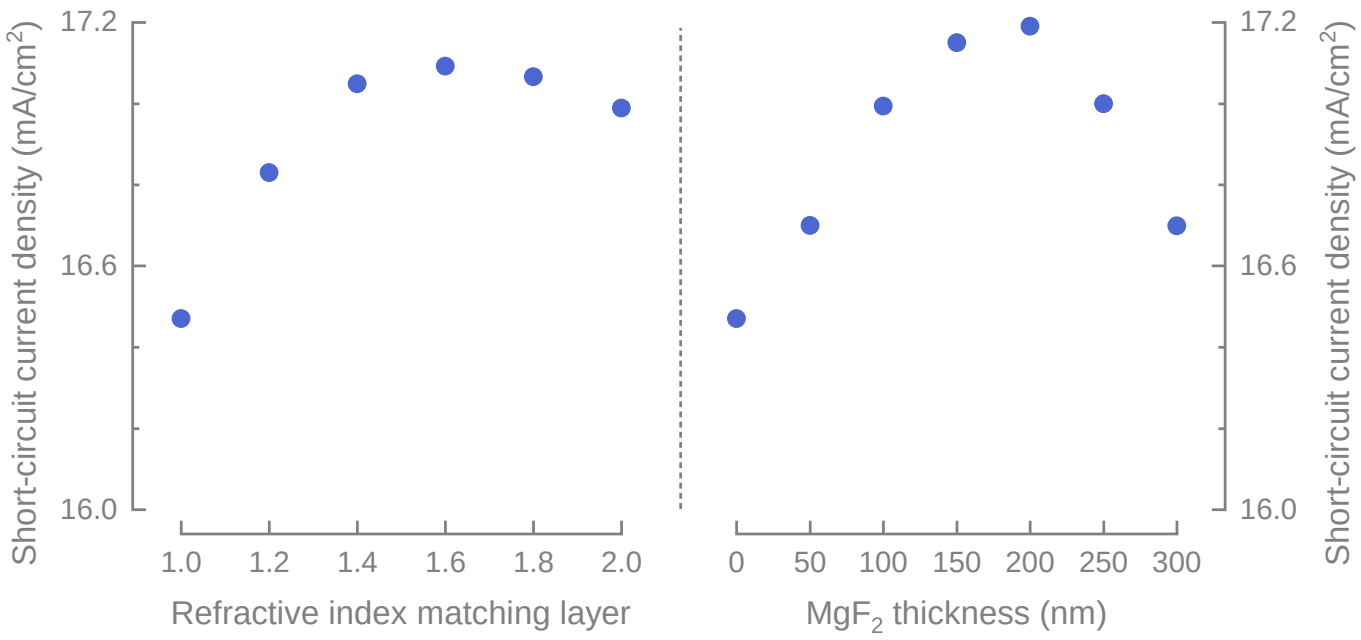

Figure 3 Simulated short-circuit current density of silicon bottom solar cell in a perovskite-silicon multijunction solar cell as a function of refractive index of intermediate medium without a MgF_2 layer (left) and thickness of MgF_2 layer without a refractive index medium, just air (right).

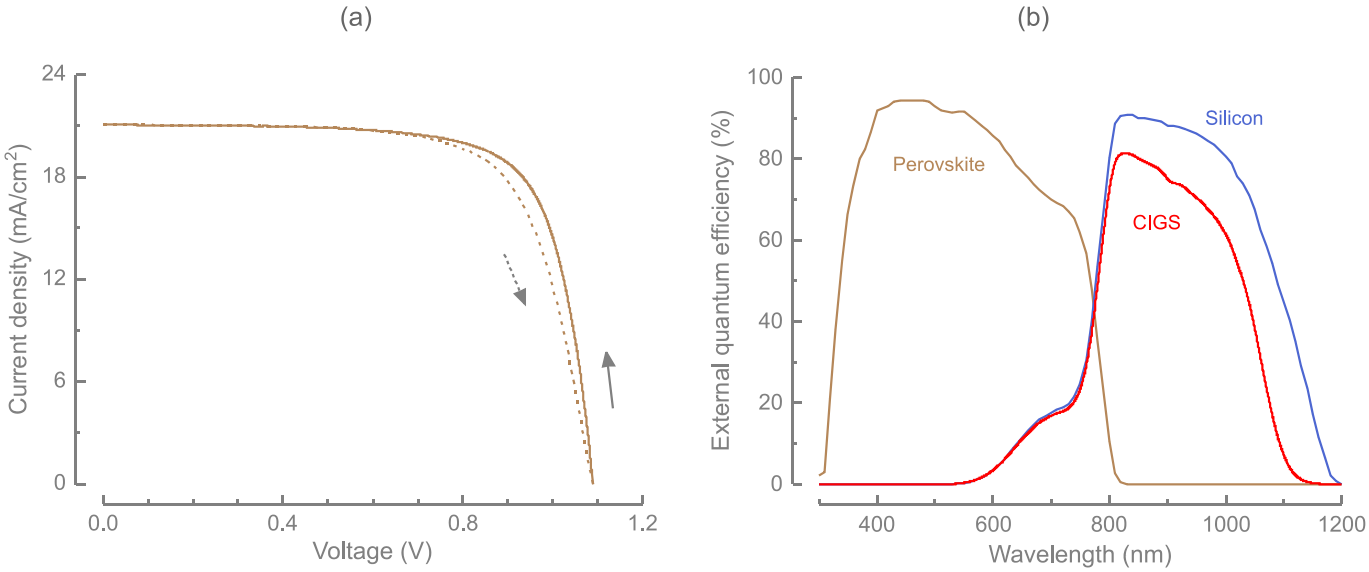

Figure 4 (a) Current density – voltage characteristics of 0.13 cm^2 semi-transparent perovskite solar cell measured using an appropriate aperture and (b) external quantum efficiency of perovskite top solar cell, CIGS and silicon bottom solar cells in four-terminal configuration.

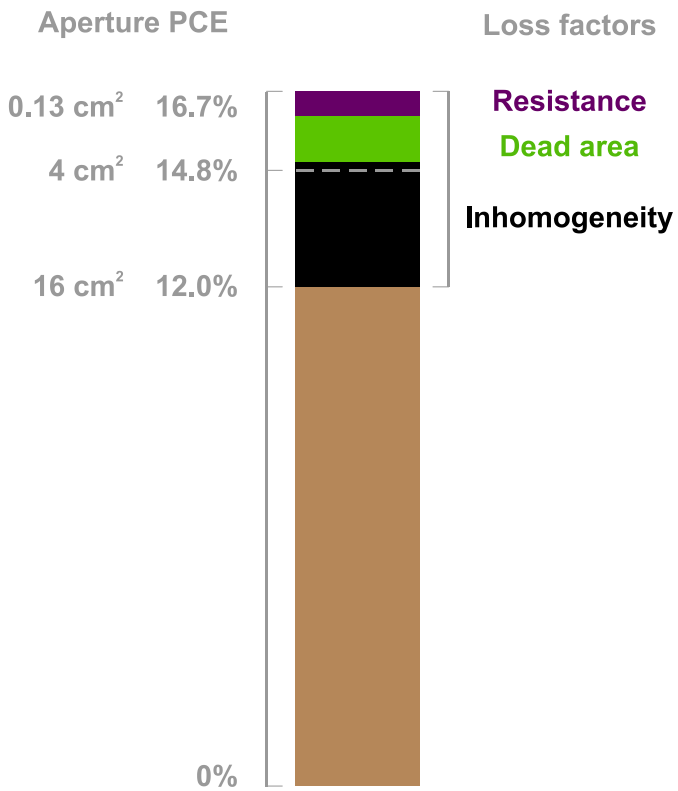

Figure 5 Illustration of different loss factors causing the decrease in aperture PCE of semi-transparent perovskite device from 0.13 cm^2 cell to 16 cm^2 module.

Table 1 Absorption of front transparent conductive oxide (TCO) of semi-transparent perovskite solar cell

Front TCO	Absorption in terms of integrated photocurrent density (mA/cm^2)	
	300 – 800 nm	800 – 1200 nm
Commercial ITO	1.52	2.73
In-house ITO	0.62	0.11

Table 2 Photovoltaic parameters of semi-transparent perovskite (with in-house front and rear ITO), CIGS, silicon solar cells and modules in four-terminal configuration. All measurements of silicon and CIGS devices are measured with the incident light filtered through a semi-transparent perovskite top solar module. The reported power conversion efficiency, PCE_{SPO}, is the stabilized power output tracked at maximum power point for 10 minutes. The PCE_{SPO} of the multijunction devices (marked with *) are calculated by adding the PCE_{SPO} of the perovskite and the corresponding bottom cell.

Device	Aperture area (cm^2)	I_{SC} (mA)	J_{SC} (mA/cm^2)	V_{OC} (V)	Fill factor (%)	Aperture PCE_{SPO} (%)
Perovskite	0.13		21.1 ± 0.15	1.07 ± 0.04	72.3 ± 0.9	16.7 ± 0.1
	4	11.1 ± 0.1	19.4 ± 0.1	7.595 ± 0.01	70.1 ± 1.1	14.8 ± 0.1
	16	20.8 ± 0.2	16.9 ± 0.2	13.65 ± 0.02	67.6 ± 1.6	12.0 ± 0.2
Silicon	4		16.9 ± 0.04	0.675 ± 0.002	81.3 ± 0.1	9.3 ± 0.01
	16	131.2 ± 0.04		1.324 ± 0.003	75.4 ± 0.2	8.2 ± 0.01
Perovskite-silicon multijunction	0.13					26.0 ± 0.1*
	4					24.1 ± 0.1*
	16					20.2 ± 0.2*
CIGS	3.8	13.1 ± 0.08		2.692 ± 0.009	75.6 ± 1.0	7.1 ± 0.05
Perovskite-CIGS multijunction	0.13					23.8 ± 0.1*
	3.8					21.3 ± 0.1*